Post-main-sequence evolution of A star debris discs

A. Bonsor[★] and M. Wyatt

Institute of Astronomy, University of Cambridge, Madingley Road, Cambridge CB3 0HA

ABSTRACT

While the population of main-sequence debris discs is well constrained, little is known about debris discs around evolved stars. This paper provides a theoretical framework considering the effects of stellar evolution on debris discs, particularly the production and loss of dust within them. Here, we repeat a steady-state model fit to disc evolution statistics for main-sequence A stars, this time using realistic grain optical properties, then evolve that population to consider its detectability at later epochs. Our model predicts that debris discs around giant stars are harder to detect than on the main sequence because radiation pressure is more effective at removing small dust around higher luminosity stars. Just 12 per cent of the first ascent giants within 100 pc are predicted to have discs detectable with *Herschel* at 160 μm. However, this is subject to the uncertain effect of sublimation on the disc, which we propose can thus be constrained with such observations. Our model also finds that the rapid decline in stellar luminosity results in only very young white dwarfs having luminous discs. As such systems are on average at larger distances they are hard to detect, but we predict that the stellar parameters most likely to yield a disc detection are a white dwarf at 200 pc with cooling age of 0.1 Myr, in line with observations of the helix nebula. Our model does not predict close-in (<0.01 au) dust, as observed for some white dwarfs; however we find that stellar wind drag leaves significant mass ($\sim 10^{-2}\,M_{\oplus}$), in bodies up to ~ 10 m in diameter, inside the disc at the end of the asymptotic giant branch (AGB) phase which may replenish these discs.

Key words: circumstellar matter – planetary systems – white dwarfs.

1 INTRODUCTION

The first dusty disc around a main sequence (MS) star was observed in 1984 around Vega (Aumann et al. 1984). Since then our knowledge of such systems has improved significantly, and it is now known that 32 per cent of A stars exhibit excess emission in the infrared, over and above the stellar photosphere (Su et al. 2006). This is thermal emission from dust particles orbiting the star in a debris disc. Debris discs are collisionally dominated in that the smallest bodies in the system are continuously replenished by collisions between larger objects and are subsequently removed by radiation pressure. The long-term evolution of such systems can be modelled by steady-state collisional models (Kenyon & Bromley 2004; Wyatt et al. 2007; Krivov et al. 2008; Kennedy & Wyatt 2010). Discs are depleted due to collisional erosion and are expected to show a slow decline in brightness. A decrease in brightness with age is indeed observed (Su et al. 2006), and can be well fitted with the models of Wyatt et al. (2007), allowing such models to characterize the population of MS A stars debris discs reasonably accurately. These models assume that velocities in the disc are high

enough that collisions are destructive. This requires that the disc is stirred, for example by self-stirring (e.g. Kenyon & Bromley 2004) or planet stirring (e.g. Mustill & Wyatt 2009).

Dust is also seen around some post-MS stars. In some cases this dust can be a result of the evolution of the star, for example material emitted in the stellar wind form spherical shells of dust that are observed around asymptotic giant branch (AGB) stars (e.g. Olofsson et al. 2010) or even stable discs observed around post-AGB stars, possibly linked to binarity (e.g. van Winckel et al. 2009). Infrared excess observed around giant stars (e.g. Jura 1999), and the helix nebula (Su et al. 2007), on the other hand, has been interpreted as a disc similar to debris discs on the MS (although alternative interpretations do exist; see e.g. Kim, Zuckerman & Silverstone 2001). Hot dust is also observed in small radii (<0.01 au) discs around white dwarfs (WDs; see e.g. Farihi, Jura & Zuckerman 2009 or von Hippel et al. 2007), again inferred to originate from a debris disc. However, in contrast to MS debris discs, these discs cannot be in steady state since material at such small radii has a short lifetime. Rather models suggest that these discs are formed when an asteroid approaches close to the star where it is tidally disrupted (Jura 2008).

There are not yet enough observations of discs around post-MS stars to fully understand the population, and it is not clear how the

[★] E-mail: abonsor@ast.cam.ac.uk

few discs that have been discovered around post-MS stars relate to the progenitor population of debris discs on the MS. In this work, we take advantage of the fact that the MS debris disc population around A stars is well characterized and extend the steady-state collisional evolution models to consider the changes to this known population during the star's evolution. In particular, we consider its detectability on the post-MS and therefore whether the observed post-MS discs derive from this population and what future observations would be best suited to detect them.

Previous work has looked at specific aspects of the effects of stellar evolution on asteroids or comets, such as stellar wind drag (Dong et al. 2010) and sublimation (Jura 2004, 2008). Dong et al. (2010) model the evolution of a planetesimal belt due to stellar mass loss and suggest that the capture of km-sized planetesimals into mean motion resonance could explain systems such as the helix nebula. In this work a theoretical framework is built that incorporates the effect of collisions, radiation forces, the stellar wind, sublimation and realistic optical properties of dust, during the star's evolution from the MS to the WD phase, focusing on the observable properties of the belt. The dynamical effects of stellar evolution, in particular stellar mass loss, on planetary systems will be considered in future work.
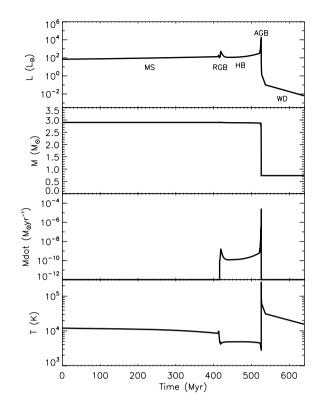
This paper begins by discussing the evolution of the star in Section 2. In Section 3, we revisit the initial population of debris discs around MS A stars, this time reproducing the fit to *Spitzer* observations at 24 and 70 μm of Wyatt et al. (2007) using a model that incorporates the optical properties of realistic grains rather than a blackbody approximation. The steady-state collisional models of Wyatt et al. (2007) are then extended to include post-MS stellar evolution. In Section 4, the changes to the properties of an individual disc, as the star evolves, are described, whilst Section 5 discusses the implications for observations of the population of debris discs around evolved stars, focusing in particular on giant stars and WDs, and Section 6 summarizes the models discussed.

2 STELLAR EVOLUTION

Knowledge of the evolution of the star is required in order to model the post-MS evolution of the debris disc. The two crucial parameters that determine the disc's evolution and detectability are the stellar luminosity and mass. In this work stellar evolution models from Hurley, Pols & Tout (2000) are used. These models use analytic formulae and are designed for population synthesis. They are accurate to within 5 per cent of more detailed models.

Here, we consider stellar evolution models for stars of mass 1.67 to 3.8 $M_\odot$; these correspond to stars of spectral type A9–B8, according to the models of Kurucz (1979), although the stellar temperature varies along the MS and a star of a given mass will be classified differently depending on the point in its evolution at which it is observed.

The evolution of A stars can be split up into various phases (see Fig. 1 for the evolution of an 2.9 $M_\odot$ star, equivalent to spectral type A0). Along the MS, the star is stable and powered by core hydrogen burning. There is a slight increase in luminosity, as the size of the hydrogen burning core increases, but mass loss is negligible. MS luminosities, for the spectral-type stars considered, range from 7.5 $L_\odot$ (1.67 $M_\odot$) to 180 $L_\odot$ (3.8 $M_\odot$) and MS lifetimes from 200 Myr (3.8 $M_\odot$) to 2000 Myr (1.67 $M_\odot$). Changes in stellar properties along the MS are negligible and therefore are ignored in Wyatt et al. (2007) and Section 3. Once hydrogen in the core is exhausted, hydrogen shell burning commences and the star swells to become a red giant branch (RGB). Its luminosity increases by

Figure 1. The luminosity (*L*), mass (*M*), mass-loss rate and temperature (*T*) evolution of a 2.9 $M_\odot$ star, $Z = 0.02$, in solar values. MS: main sequence (0–413 Myr); RGB: red giant branch (415.9–418.7 Myr); HB: horizontal branch (418.7–521.4) Myr; AGB: asymptotic giant branch (521.4–525.9) Myr; WD: white dwarf (525.9 Myr onwards).

several orders of magnitude. The RGB phase lasts for ~10 Myr, until core temperatures are hot enough that helium burning starts, possibly degenerately in a helium flash (for $M \leq 2.25\,M_\odot$), after which its luminosity decreases. For those stars where helium burning starts degenerately, the star reaches a higher luminosity on the RGB than for higher mass stars. This means that although the initial luminosity on the giant branch increases with stellar mass, the value at the tip of the giant branch has a minimum for stars that no longer start helium burning degenerately ($M \geq 2.25\,M_\odot$), increasing up to ~$10^4\,L_\odot$ for 1.67 $M_\odot$ stars. The star's luminosity increases slowly as it moves along the horizontal branch (HB), which lasts for ~100 Myr. Once helium in the core is exhausted the star swells to become an AGB star and its luminosity increases yet further. Luminosities of evolved A stars can reach up to $2 \times 10^4\,L_\odot$ for a 3.8 $M_\odot$ star in this phase.

The majority of mass loss occurs on the AGB. There is a fair degree of uncertainty in mass-loss rates and the exact mechanism driving the mass loss in AGB stars (see review by Willson 2000). The stellar evolution code uses the mass loss of Kudritzki & Reimers (1978) on the RGB and HB:

$$\dot{M}_R = 2 \times 10^{-13} \frac{L_* R_*}{M_*} \, M_\odot \, yr^{-1}, \qquad (1)$$

where M_*, R_* and L_* are the stellar mass, radius and luminosity in solar values.

On the AGB the formulation of Vassiliadis & Wood (1993) is used:

$$\log \dot{M}_{VW} = -11.4 + 0.0125$$
$$\times [P - 100 \max(M_* - 2.5, 0.0)]\, M_\odot \, yr^{-1} \qquad (2)$$

$$P = \min(3.3, -2.07 - 0.9 \log M_* + 1.94 \log R_*) \qquad (3)$$

where P is the Mira pulsation period of the star, in days. The expansion velocity for the stellar wind is given by

$$v_{SW} = -13.5 + 0.056P \quad km\, s^{-1}. \qquad (4)$$

The mass-loss rate peaks in a superwind phase, at the tip of the AGB (Vassiliadis & Wood 1993), with

$$\dot{M} = 1.36 \times 10^{-9} L_*\, M_{\odot}\, yr^{-1}. \qquad (5)$$

These are empirical mass-loss rates, fitted to observations of RGB and AGB stars. Thermal pulses, with periods $\sim 10^5$ yr, dominate the evolution on the AGB as the star switches between helium and hydrogen shell burning. This may lead to discrete superwind phases and the multiple shells seen in many planetary nebulae.

The WD core now evolves at constant luminosity to higher effective temperature. This luminosity is proportional to the WD mass. The hotter radiation from the WD core ionizes the expelled gas which is seen as a planetary nebula. Once the WD core reaches a maximum effective temperature it starts cooling at constant radius. The radiative cooling of the WD is modelled by the Mestel theory (Mestel 1952), with the WD luminosity, in solar units, given by

$$L_{WD} = \frac{635 M_{WD} Z^{0.4}}{[A(t+0.1)]^{\alpha}} \qquad (6)$$

where M_{WD} is the mass of the WD ($M_{\odot}$), Z is the metallicity, t is the cooling age or time since the WD formed, in Myr, and A is a parameter that is composition dependent. In the current models solar metallicity, $Z = 0.02$ and $A = 15$ for a CO WD is used. Once the WD has cooled significantly, crystallization occurs, and the cooling rate enters a different phase, and hence in these models α changes from 1.18 to 6.48 at an age of 9 Gyr, for all spectral types. Although prescriptions for WD crystallization have improved significantly since the groundbreaking work of Mestel (1952) (see e.g. Metcalfe, Montgomery & Kanaan 2004), however crystalization only occurs when the WD cools to $\sim$6000–8000 K (Metcalfe et al. 2004) and therefore Mestel (1952) should provide accurate luminosities for WDs hotter than this. It is found later in this work that debris discs are only detectable around very young, hot WDs (see Section 5.2.3) and therefore differences between the cooling theory of Mestel (1952) and more modern prescriptions are not significant for the current work.

3 STEADY-STATE MODELS FOR POPULATION OF DEBRIS DISCS AROUND MAIN-SEQUENCE A STARS

3.1 Evolution of an individual disc

The evolution of an individual disc, due to collisions, can be described by a simple steady-state model such as that presented in Wyatt et al. (2007). These models assume that the size distribution of all particles is the same as for an infinite collisional cascade:

$$n(D)dD \propto D^{-7/2} dD. \qquad (7)$$

This size distribution holds from the largest planetesimals of size, D_c, down to the smallest dust grains present of size, D_{min}, and assumes that all bodies of all sizes have the same strength per unit mass. In the steady-state models for MS stars D_{min} is determined by the largest grains that are not blown out of the system by radiation pressure, the blow-out size (D_{bl}). The blow-out size is an important property of the system and depends on the stellar parameters. Assuming spherically symmetric blackbody grains, of uniform density ρ in kg m^{-3}, it is given, in µm by (Burns, Lamy & Soter 1979)

$$D_{bl} = 0.8 \left(\frac{L_*}{M_*}\right) \left(\frac{2700}{\rho}\right), \qquad (8)$$

where L_* and M_* are the stellar luminosity and mass in solar units.

For such a cascade, the majority of the cross-sectional area of the disc is found in the smallest particles, but the mass of the disc is determined by the largest objects. In these models the evolution of the mass in the disc (M_{tot} in $M_{\oplus}$) is determined by the collisional lifetime (t_c) of the largest objects, with diameter, D_c, in km:

$$\frac{dM_{tot}}{dt} = \frac{-M_{tot}}{t_c(D_c)}. \qquad (9)$$

The collisional lifetime of particles of diameter D_c was determined in Wyatt et al. (2007) and is given by

$$t_c = 5.20 \times 10^{-13} \frac{\rho\, r^{13/3} \left(\frac{dr}{r}\right) Q_D^{*5/6} D_c}{M_{tot} M_*^{4/3} e^{5/3}} \quad Myr, \qquad (10)$$

where r is the radius of the disc, in au, and dr is the width of the disc, taken to be $\frac{r}{2}$, e is the eccentricity of the particles, assumed to be equal to their inclination I, Q_D^* is the dispersal threshold for collisions in J kg^{-1} and ρ is the density of particles, taken to be 2700 kg m^{-3}. So long as the only time-dependent variable in equation (9) is the mass in the disc, it can be shown that the mass in the disc evolves as

$$M_{tot}(t) = \frac{M_{tot}(0)}{(1 + \frac{t}{t_c})}. \qquad (11)$$

For early times, when $t \ll t_c$, the mass in the disc remains approximately constant at its initial value, only turning over and falling off as $M_{tot} \propto \frac{1}{t}$ at times $t \gg t_c$. At late times (t in Myr) the mass in the disc tends to a value M_{max} that is independent of its initial value,

$$M_{max}(t) = 5.2 \times 10^{-13} \frac{\rho\, r^{13/3} \left(\frac{dr}{r}\right) Q_D^{*5/6} D_c}{M_*^{4/3} e^{5/3} t} \quad M_{\oplus}. \qquad (12)$$

These models are, however, a simplification. It is only considered that collisions between the largest bodies change the mass in the disc. Only a single value for the dispersal threshold, Q_D^*, is used and cratering collisions (e.g. Kobayashi & Tanaka 2010) are ignored. However, this simple procedure allows us to fit the observations. The calculated dust luminosities are within an order of magnitude of more detailed prescriptions in which collisions between all diameter particles are considered, Q_D^* is a function of diameter and the size distribution is three-phase, for example (Löhne, Krivov & Rodmann 2008).

In Wyatt et al. (2007), the emission properties of the disc were calculated using a blackbody approximation. For reasons that are explained in Section 4.4.1, a blackbody approximation cannot be used in the current models. The models of Wyatt et al. (2007) were updated to incorporate realistic emission properties of grains using the method of Wyatt & Dent (2002). The prescription of Li & Greenberg (1997) was used to calculate optical properties for grains with a composition of 1/3 silicates, 2/3 organic refractory materials and zero porosity, using the Mie theory, the Rayleigh–Gans theory or geometric optics in the appropriate limits. The temperature in the disc now depends on the particle's diameter, D, in addition to its distance from the star, r in au:

$$T(D, r) = \left(\frac{\langle Q_{abs} \rangle_{T_*}}{\langle Q_{abs} \rangle_{T(D,r)}}\right)^{1/4} T_{bb} \qquad (13)$$

where $\langle Q_{abs}\rangle_{T_*}$ and $\langle Q_{abs}\rangle_{T(D,r)}$ are the particle's absorption efficiency averaged over the stellar spectrum and the spectrum of a blackbody radiating at temperature, T, and T_{bb} is the equilibrium temperature of the particle if it were a blackbody, given by

$$T_{bb} = 278.3 \frac{L_*^{1/4}}{r^{1/2}} \quad \text{K},$$

where L_* is the star's luminosity in solar units. The flux from the disc, at a wavelength λ, is given by

$$F_{disc}(\lambda) = 2.98 \times 10^{-7} \frac{P(\lambda, r)M_{tot}}{\sqrt{D_{min}}D_c\rho d^2} \quad \text{Jy}, \tag{14}$$

where M_{tot} is the mass in the disc in $M_\oplus$, $D_{min}(\mu m)$ and D_c (km) are the smallest and the largest particles in the disc, ρ is the density of particles, in kg m^{-3}, d is the distance from the observer to the star, in pc,

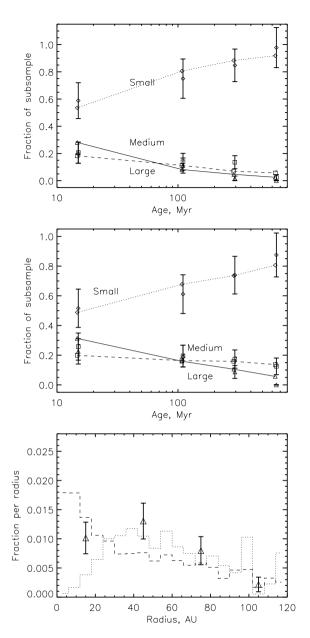$$P(\lambda, r) = \int_{D_{min}}^{D_c} Q_{abs}(\lambda, D)B_\nu(\lambda, T(D, r))\bar{\sigma}(D)dD, \tag{15}$$

where $B_\nu(\lambda, T(D, r))$ is the blackbody flux, in Jy Sr^{-1}, and $\bar{\sigma}(D)dD$ is the proportion of the total cross-section of the disc found in particles with sizes between D and $D + dD$.

3.2 Population of discs around A stars

The population of debris discs around MS A stars (spectral type B8 to A0) is relatively well constrained from observations by *Spitzer* at 24 and 70 μm (Rieke et al. 2005; Su et al. 2006). Rieke et al. (2005) searched a sample of 76 individual A stars, with ages between 0 and 800 Myr, for excess with *Spitzer* at 24 μm. This was extended by looking at archival *IRAS* data to a total of 266 stars. Su et al. (2006) search a sample of 160 stars for excess at both 24 and 70 μm. Fig. 2 plots the stars that were found to have infrared excess in both surveys. Fig. 2 plots the fraction of stars in different age bins that are classified to have small, medium or large levels of excess. The level of excess decreases with stellar age at both wavelengths, but at a faster rate at 24 μm.

The models in Wyatt et al. (2007) were fitted to these observations, using a population of 10 000 discs, with a distribution of initial masses, radii, spectral type, distance and ages. The initial masses formed a lognormal distribution centred on M_{mid}, assuming the same width as for proto-planetary discs, 1.14 dex (Andrews & Williams 2005) and the initial radii a power-law distribution, with the number of discs with radius between r and dr given by $N(r)dr \propto r^{-\gamma}dr$, for discs between r_{min} and r_{max}. It was assumed that the stars are randomly distributed evenly in spectral type and age and isotropically in distance. In the original model, the dust properties were assumed to be blackbody like and the 24 and 70 μm statistics were fitted by adjusting the parameters M_{mid}, D_c, e, Q_D^*, γ, r_{min} and r_{max}.
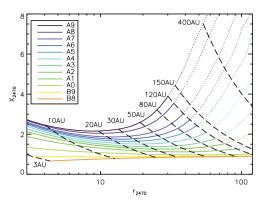
Here we repeated the fit, using the updated formulation that incorporates the optical properties of realistic grains, to find new values for this parameter set. As discussed in Wyatt et al. (2007), a degeneracy in the model means that these parameters are not uniquely constrained. The fit to the data is good so long as both $D_c^{1/2}Q_D^{*,5/6}e^{-5/3}$ (equation 15 of Wyatt et al. 2007) and $M_{tot,mid}D_c^{-1/2}$ (equation 16 of Wyatt et al. 2007) remain constant. The former can be explained by the example of a massive disc composed of stronger bodies that evolves on the same time-scale as a less massive disc of weaker bodies. Alternatively, the latter can be explained by the fact that a massive disc that contains more of its mass in larger bodies (i.e. a larger value for D_c) has the same dust mass and therefore is equivalently bright as a less massive disc where D_c is smaller. Here, we

Figure 2. Upper and middle panels: the fit to the observations of Su et al. (2006) at 24 (upper) and 70 μm (middle), comparable to fig. 2 of Wyatt et al. (2007). The plots show the fraction of stars with flux ratios in different age bins (<30 Myr, 30–190 Myr, 190–400 Myr), at 24 μm $\frac{F_{disc}}{F_*} = 1$–1.25 (diamond: small excess), 1.25-2 (square: medium excess), >2 (triangle: large excess) and similarly at 70 μm $\frac{F_{disc}}{F_*} = 1$–5 (diamond: small excess), 5–20 (square: medium excess), >20 (triangle: large excess). Observed values are shown with $\sqrt{N}$ error bars, whilst model values are joined with dotted, dash and solid lines, for small, medium and large excess. Lower: the distribution of planetesimal belt radii. The model population is shown with a dashed line, whilst the sub-sample of the model population that is detectable at both 24 and 70 μm is shown with a dotted line. The observed distribution of radii is shown with triangles and $\sqrt{N}$ error bars.

chose to keep Q_D^* and e unchanged at 150 J kg^{-1} and 0.05, respectively, without any loss of generality and performed a fit to M_{mid}, D_c, γ, r_{min} and r_{max}.

In order to fit the observations with a new population calculated using the emission properties of realistic grains, we want every disc to evolve in the same way as every disc in the old population, calculated using a blackbody approximation. The optical properties

Figure 3. The ratio of the radius (r) of a disc calculated using realistic grains to the radius inferred from the flux at 24 and 70 μm, assuming blackbody emission (r_{2470}), as a function of r_{2470}.

Table 1. Parameter values for the original models from Wyatt et al. 2007 and the new values calculated in this work.

Parameter	Original value	New value
M_{mid}	10.0	7.8 $M_\oplus$
D_c	60.0	1.9 km
e	0.05	0.05
Q_D^*	150 Jkg^{-1}	150 Jkg^{-1}
γ	0.8	0.8
r_{min}	3 au	6 au
r_{max}	120 au	250 au

of realistic grains mean that they are hotter and emit less efficiently at longer wavelengths. Therefore, in order for the flux ratio $\frac{F_{disc,24\,\mu m}}{F_{disc,70\,\mu m}}$ to remain the same, disc radii must increase. In fact, a good fit is achieved by adjusting the disc radii from the values in the original model, $r2470$, to a new value, $r = X_{2470}r_{2470}$, so long as the other parameters are also adjusted accordingly; thus we keep γ at 0.8, whilst r_{min} and r_{max} increase by a factor of X_{2470}. Then, in order to keep the flux from each disc constant, its fractional luminosity (f), the ratio of the luminosity of the disc to the luminosity of the star, should remain unaltered. Grains are larger than the emission wavelength of starlight on the MS such that they absorb starlight efficiently and $f \propto \frac{M_{tot}}{r^2 D_c^{1/2} D_{min}^{1/2}}$. Therefore, we need to adjust M_{tot} and D_c keeping $\frac{M_{tot}}{\sqrt{D_c}r^2}$ constant. The maximum fractional luminosity that a disc of a given age can have due to its collisional evolution should also remain constant and thus using equation (12) $r^{7/3}D_c^{1/2}$ is also a constant. Together these mean that D_c and M_{mid} are altered by $X_{2470}^{-14/3}$ and $X_{2470}^{-1/3}$, respectively.

The conversion between r and r_{2470} was determined for realistic grains with the prescribed size distribution around MS stars and is shown in Fig. 3. There is a functional dependence of X_{2470} on r_{2470} and spectral type that can be readily understood. For a given spectral type, X_{2470} has a minimum at intermediate radii but increases at small and large radii. The latter arises because the cooler temperatures at larger radii mean that the emission at these wavelengths is on the Wien side of the blackbody spectrum. This means that the small increase in the temperature of the grains causes a larger increase in the flux ratio at these wavelengths and hence the radius inferred, r_{2470}. This is compounded by the fact that the temperature of blow-out grains falls off more slowly with radius than that of blackbody grains (e.g. Su et al. 2009). The increase at small radii arises because the emission efficiency of realistic grains falls off with wavelength, such that the emitted spectrum appears steeper (i.e. hotter) than the true grain temperatures. This effect is more important where the spectrum is steeper, i.e. where discs are hotter. All of these effects are more pronounced for later spectral-type stars because the blow-out size is smaller (equation 8) and therefore there is a larger population of grains whose properties depart from blackbody.

X_{2470} was found self-consistently using Fig. 3 to give an average value of 2.1. The above discussion suggests that an equally good fit to the statistics could be obtained with $M_{mid} = 7.8\,M_\oplus$ and $D_c = 1.9$ km, as shown in Table 1. Indeed, as is shown in Fig. 2, this is found to be the case, with a total $\chi^2_{24,70,r}$ of 16.0 compared to 9.8 of Wyatt et al. (2007).

4 MODELS OF DEBRIS DISCS AROUND POST-MAIN-SEQUENCE A STARS

The steady-state models for the evolution of the disc due to collisions described in Section 3 are extended to include the effects of the evolution of the star, described in Section 2. The evolution of individual discs and changes to their properties are discussed. Individual discs follow different evolutionary paths depending on their properties. The plots presented in this section are representative, and look at the evolution of a disc around a 2.9 $M_\odot$ (equivalent to A0) star, with solar metallicity ($Z = 0.02$), initial masses in the disc of 1.0, 10.0 and 100.0 $M_\oplus$, and initial radii of 10, 50 and 100 au, although the population models discussed in Section 5.2 use the evolution for the appropriate disc and stellar parameters.

4.1 Radius evolution

As the star loses mass, the semimajor axes of orbiting bodies will increase. The star loses the majority of its mass in 10^5 yr at the tip of the AGB. For the majority of discs, this mass-loss time-scale is much longer than the orbital time-scales of particles, and therefore the mass loss can be considered to be adiabatic. Only for the discs at much larger radii do the orbital time-scales start to approach the mass-loss time-scales and the assumption of adiabatic mass loss may break down, inducing eccentric orbits, for example a body initially in a circular orbit at 100 au will gain an eccentricity of 0.1 if mass-loss rates reach $10^{-4}\,M_\odot\,yr^{-1}$.

However, these effects are small and are ignored in the current models, where the evolution of the radius (r) due to adiabatic mass loss is given by Villaver & Livio (2007)
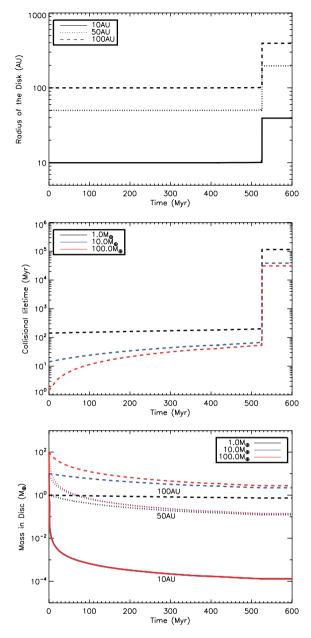
$$r(t) = \frac{r(0)M_*(0)}{M_*(t)}. \tag{16}$$

Essentially, the radius of the disc switches from an initial to a final value during the $\sim 10^5$ yr of extreme mass loss, at the tip of the AGB, as shown in the upper panel of Fig. 4.

4.2 Mass in the disc and the collisional lifetime

As discussed in Section 3, the mass in the disc is dominated by the largest particles, and hence the time-scale on which the mass is depleted is dependent on the collisional lifetime of the most massive particles, t_c (equation 10). The evolution of t_c is shown in the middle panel of Fig. 4. Collisions occur most frequently (t_c is shorter) in the most massive discs, closest to the star. The collisional lifetime increases significantly when the star loses mass, and is given by

$$t_c = \frac{t_c(0)M_{tot}(0)M_*^{17/3}(0)}{M_*(t)^{17/3}M_{tot}(t)}. \tag{17}$$

Figure 4. The evolution of the disc radius (upper), collisional lifetime (middle) and total disc mass (lower) for different initial disc masses, $1.0\,M_\oplus$ (black), $10.0\,M_\oplus$ (blue), $100.0\,M_\oplus$ (red), and radii 100 au (dashed line) [bottom plot only 50 au (dotted line), 10 au (thick line)] around a $2.9\,M_\odot$ star.

Once the mass in the star changes as a function of time, the evolution of the mass in the disc is no longer given simply by equation (9), instead

$$\frac{dM_{tot}}{dt} = \frac{-M_{tot}}{t_c} \propto \frac{M_{tot}^2(t)M_*^{4/3}(t)}{r^{13/3}(t)}. \tag{18}$$

Using the expression for $r(t)$,

$$\int \frac{dM_{tot}}{M_{tot}^2} \propto \int M_*^{17/3}dt. \tag{19}$$

Therefore,

$$M_{tot} = \frac{M_{tot}(0)}{1 + M_{tot}(0)K \int M_*^{17/3}dt} \tag{20}$$
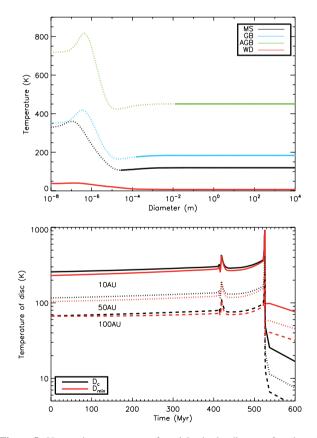
where

$$K = \left[1.4 \times 10^{-9} \left(\frac{dr}{r}\right) e^{-5/3} D_c Q_D^{*5/6} r(0)^{13/3} M_*(0)^{13/3}\right]^{-1}. \tag{21}$$

However the mass in the star is approximately constant until the AGB, and up until this point equation (9) is valid. In fact up to the end of the AGB, the evolution of the mass in the disc is similar to that on the MS in that M_{tot} remains approximately constant for discs with longer collisional lifetimes (larger radii) and tends to M_{max} (equation 12) for discs with shorter collisional lifetimes (small radii), as shown in the bottom panel of Fig. 4. Once the star loses mass on the AGB, the collisional lifetime of larger objects increases so much that it approaches the Hubble time, even for close-in discs (see the middle panel of Fig. 4). Collisional evolution is no longer significant for the total disc mass, which remains constant throughout the WD phase.

4.3 Temperature of the disc

Particles in the disc are heated by stellar radiation. Their temperature is a balance between absorption and emission and is a function of particle diameter, as shown in the upper panel of Fig. 5. Large grains emit efficiently and act like blackbodies, whilst medium-sized

Figure 5. Upper: the temperature of particles in the disc as a function of particle diameter, for a disc initially at 50 au around a $2.9\,M_\odot$ star, around a MS star ($L_* = 190\,L_\odot$), giant star ($L_* = 500\,L_\odot$), an HB star ($L_* = 150\,L_\odot$), an AGB star ($L_* = 1.5 \times 10^4\,L_\odot$) or white dwarf ($L_* = 7 \times 10^{-3}\,L_\odot$). The solid lines show bound grains that are included in the model, whereas the dotted lines are unbound grains that are excluded from the model. Lower: the evolution of the temperature of blackbody grains (D_c) and the smallest grains in the disc (D_{min}), for discs initially at 10 au (thick line), 50 au (dotted line), 100 au (dashed line) around a $2.9\,M_\odot$ star.

grains ($\sim$ μm) emit inefficiently and are therefore hotter than blackbody. The smallest ($<$ μm) grains emit and absorb inefficiently and reach a temperature that is independent of grain size.

To illustrate the evolution of the temperature of particles in the disc we show in the lower panel of Fig. 5 the change in the temperature of blackbody particles (appropriate for large grains) and the smallest grains in the disc of size D_{min} (as calculated in Section 4.4) as the star evolves. This follows the luminosity of the star. Along the MS the temperature of the disc is relatively constant, but it increases up to several hundred kelvin (depending on disc radius) as the star's luminosity increases on the RGB and AGB. The temperature of the disc falls dramatically as the star becomes a WD, mostly because the stellar luminosity drops by several orders of magnitude, but also because the discs are now further from the star. For this example mass star, the only epoch when the temperature of any particle in the disc greatly exceeds the blackbody temperature is for WDs; however for later spectral type (lower mass) stars the smaller grains may be hotter than blackbody through all phases of stellar evolution.

4.4 Smallest particles in the disc

The size of the smallest particles (D_{min}) in the collisional cascade was determined in the Wyatt et al. (2007) models and in Section 3 by radiation pressure (the blow-out size equation 8). This is correct for most discs around MS stars; however there are several other forces that can remove small particles from the disc, including the Poynting–Robertson (PR) drag, stellar wind pressure, stellar wind drag and sublimation. In the models presented here, D_{min} is determined by whichever of these removes the largest diameter objects at a given epoch. In the following section all five processes are discussed and compared such that D_{min} can be determined for every disc during its evolution. The outcome is summarized in Fig. 6.
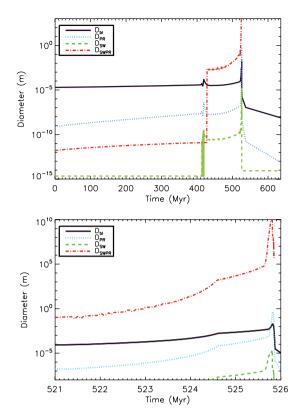
4.4.1 Radiation pressure

Radiation pressure is a radial force which acts in the opposite direction to the star's gravity. The ratio of radiation forces to the gravitational forces is given by

$$\beta_{\mathrm{rad}} = \frac{F_{\mathrm{rad}}}{F_{\mathrm{grav}}} = 0.43 \frac{\langle Q_{\mathrm{pr}} \rangle L_*}{M_* D}, \tag{22}$$

where $\langle Q_{\mathrm{pr}} \rangle$ is the radiation pressure efficiency for grains of a given diameter D, in μm, averaged over the stellar spectrum. The dependence of β_{rad} on particle diameter, for realistic grains, is shown in the upper panel of Fig. 7 at different epochs. The peak in β_{rad} occurs at a size comparable to the peak wavelength in the stellar spectrum. The dotted line shows the approximation to β_{rad} used in this work for which $\langle Q_{\mathrm{pr}} \rangle = 1$. It only deviates from the more realistic calculation at the smallest particle sizes and since these small particles are generally removed from the disc, apart from during the WD phase, this is considered a reasonable approximation.

If $\beta_{\mathrm{rad}} > 1$, the radiation forces are greater than the gravitational forces and particles are unbound. However, for small particles produced in collisions radiation pressure causes their orbits to differ from that of the parent body, resulting in a hyperbolic orbit if $\beta_{\mathrm{rad}} > 0.5$ (Burns et al. 1979). Radiation pressure also causes bound grains with $0.1 < \beta_{\mathrm{rad}} < 0.5$ to have eccentricities greater than their parents. This causes a perturbation to the size distribution from that assumed in equation (7) (e.g. Strubbe & Chiang 2006; Thébault & Augereau 2007), but the resulting disc flux can be approximated by assuming the eccentricity to be constant for all particles and

Figure 6. The limiting diameter below which objects are removed by either radiation pressure (D_{bl}), Poynting–Robertson (PR) drag (D_{PR}), stellar wind pressure (D_{SW}) or stellar wind drag (D_{SWPR}), calculated using equation (8), equation (25), equation (28) and equation (30), in a disc initially at 100 au with a mass of $10\,\mathrm{M}_{\oplus}$, around an evolving $2.9\,\mathrm{M}_{\odot}$ star. The lower panel shows a zoom-in on the AGB. D_{SWPR} overestimates the diameter bodies that are removed by stellar wind drag as it does not take into account the finite AGB lifetime.

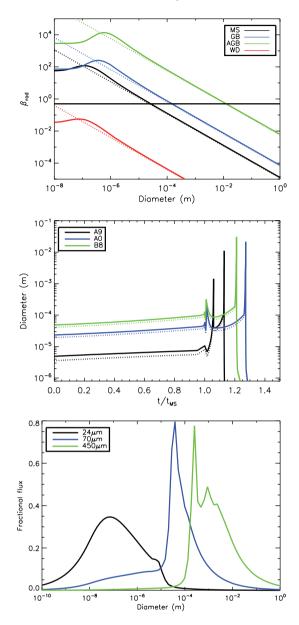ignoring the effect on the size distribution, which is assumed to be truncated at D_{bl} calculated using equation (8).

The middle panel in Fig. 7 shows how the blow-out size (D_{bl}) changes as the star evolves for stars with different initial masses. The blow-out size follows the luminosity evolution of the star, increasing on both the RGB and AGB, up to $\sim$cm in size, before decreasing significantly as the star becomes a WD. The stellar luminosity of a WD is so low that once the star has cooled sufficiently ($L_{\mathrm{WD}} \leq 0.1\,\mathrm{L}_{\odot}$), β_{rad} is never above 0.5 (as seen in Fig. 7) and no grains are removed from the system by radiation pressure. The change in stellar luminosity or β_{rad} with time causes particles to spiral inwards, changing its semimajor axis by

$$a(t) = \frac{a(0)(1 - \beta_{\mathrm{rad}}(0))}{(1 - \beta_{\mathrm{rad}}(t))}, \tag{23}$$

where $a(0)$ and $\beta_{\mathrm{rad}}(0)$ are the semimajor axis and ratio of the radiation pressure to the stellar gravity at the start of the WD phase. No particles ever reach the star by this process; the maximum fractional change in semimajor axis is $(1 - \beta_{\mathrm{rad}}(0))$.

This leaves the question of what, if anything, removes the smallest particles from collisional cascades in discs around WDs, a problem which also exists for M-dwarfs (Plavchan et al. 2009). It is possible that magnetic effects or interactions with the interstellar medium remove the smallest particles in discs around WDs. In this work, however, the fate of the smallest particles is left as an open question. The bottom panel of Fig. 7 shows that, should they exist, particles

example, even for the extreme case of a disc at 100 au, around an evolved 2.9 $M_\odot$, with a WD cooling age of 1 Myr and a size distribution that extends down to 10^{-10} m, the contribution of particles less than 10^{-8} m in size to the 24 μm disc flux is only 20 per cent. Thus for practical purposes we set $D_{min} = 10^{-8}$ m.

4.4.2 Poynting–Robertson drag

Radiation forces also oppose the velocity of an orbiting dust particle, reducing its angular momentum and causing it to spiral inwards, by the PR drag, changing its radius by order itself on time-scales of

$$t_{pr} = 1.4 \times 10^{-6} \frac{r^2 \rho D}{L_* \langle Q_{pr} \rangle} \quad \text{Myr.} \tag{24}$$

PR drag is only relevant for particle sizes for which the PR drag time-scale is significantly shorter than the collisional lifetime, since otherwise the particles are destroyed by collisions before they have had the opportunity to migrate. Assuming that the size distribution extends down in size indefinitely according to equation (7) and that PR drag lifetime varies according to equation (24), both of which are valid in the regime where radiation pressure is negligible, it is possible to derive a condition for the diameter, D_{PR}, at which the collisional cascade is truncated by PR drag, by comparing the collisional lifetime of the smallest grains to their PR-drag lifetime:

$$D_{PR} = 8.63 \times 10^{-23} \frac{L_*^2 \left(\frac{dr}{r}\right)^2 r^{7/3} Q_D^{*5/3} D_c}{M_*^{8/3} M_{tot}^2 e^{10/3}} \quad \mu\text{m.} \tag{25}$$

In Fig. 6 D_{PR} is compared to D_{bl} (equation 8). D_{PR} is always smaller than D_{bl} for the disc initially at 100 au with $10\,M_\oplus$ shown, such that collisions and radiation pressure dominate over PR drag which can therefore be ignored, as was previously shown in Wyatt (2005). A similar analysis for discs of different mass and radii around different mass stars shows that PR drag can always be ignored except for close-in discs or those low in mass.

PR drag in discs around WDs is of particular interest as a possible mechanism to remove the smallest grains. Of potential importance is the fact that objects larger than $D > \frac{22.4\,\text{mm}}{r(0)^2}$ can never reach the star due to PR drag. This is because the luminosity of the WD decreases, and thus the rate at which objects spiral in decreases with time. The critical size is calculated by solving for the rate of change of semimajor axis, a, due to PR drag, for a zero eccentricity particle, given by (Burns et al. 1979)

$$\left\langle \frac{da}{dt} \right\rangle = -\frac{3L_{WD}}{8\pi\rho c^2 Da} \tag{26}$$

where L_{WD} is given by equation (6). However since collisions still occur on faster time-scales than PR drag can act, even for the smallest particles present (10^{-8} m, as is seen in the upper panel of Fig. 6), it is not expected that PR drag has a significant effect on debris discs around WDs.

4.4.3 Stellar wind pressure

Mass loss is an important feature of stellar evolution along the giant, horizontal and AGBs; however mass-loss rates are low and do not affect the disc significantly except towards the end of the AGB. It should be noted that there is a relatively large degree of uncertainty in the exact mass-loss rates of an evolving star, as discussed in Section 2. The effect of the stellar wind on particles in the disc is very similar to that of stellar radiation in that its pressure component causes the smallest particles created in collisions to have eccentric

Figure 7. The effect of radiation pressure on the disc. Calculations with $\langle Q_{pr} \rangle = 1$ are shown with dotted lines, whilst the solid lines show a more realistic calculation. Upper: the ratio of the radiational to gravitational forces (β_{rad}) for different diameter particles in a disc around a MS star ($L_* = 190\,L_\odot$), giant star ($L_* = 500\,L_\odot$), AGB star ($L_* = 1.5 \times 10^4\,L_\odot$) or WD ($L_* = 7 \times 10^{-3}\,L_\odot$). The horizontal black line shows $\beta_{rad} = 0.5$. Particles with $\beta_{rad} > 0.5$ are removed from the system by radiation pressure. The maximum value of β_{rad} is less than 0.5 around a WD, once L_{WD} falls below $\sim 0.15\,L_\odot$. Middle: the change in the blow-out diameter of realistic grains around 1.67, 2.9 and 3.8 $M_\odot$ or A9, A0 and B8 stars. For both plots the dotted lines show calculations with $\langle Q_{pr} \rangle = 1$, which do not vary significantly from the solid lines, which include a more realistic calculation of $\langle Q_{pr} \rangle$, apart from for small diameter particles. Lower: the fraction of the flux per unit log diameter, defined such that the area under the curve is 1, for a disc at 100 au, around an evolved 2.9 $M_\odot$ star as a WD with a cooling age of 1 Myr.

smaller than $D_{min} = 10^{-8}$ m contribute negligibly to the total flux in the wavebands considered here. This is because, despite the size distribution of equation (7) meaning that such grains contain the majority of the cross-sectional area in the disc, such small grains also have extremely low emission efficiencies at longer wavelengths. For

or unbound orbits, and its drag component causes them to spiral inwards. Assuming a stationary wind model, with a constant wind velocity v_{SW}, the ratio of the pressure force due to the stellar wind to the gravitational forces is given by

$$\beta_{SW} = 5.67 \times 10^{10} \frac{\dot{M}_* v_{SW} Q_{SW}}{M_* \rho D}, \tag{27}$$

where $\langle Q_{SW} \rangle$ is the efficiency for momentum transfer from the stellar wind, assumed to be 1, $\dot{M}_*$ the mass-loss rate, in $M_\odot \, yr^{-1}$, and v_{SW} the wind velocity, in $km \, s^{-1}$.

Just like with radiation pressure grains smaller than D_{SW} or with $\beta_{SW} > 0.5$ would be removed from the system, where

$$D_{SW} = 1.13 \times 10^{-4} \frac{\dot{M}_* v_{SW}}{\rho M_*} \ \ m. \tag{28}$$

However, as shown in Fig. 6 D_{SW} is smaller than D_{bl} throughout the star's evolution, such that the removal of grains by stellar wind pressure can be ignored.

4.4.4 Stellar wind drag

The stellar wind causes particles of diameter, D, in μm, to spiral in towards the star on time-scales of

$$t_{SW} = 9.4 \times 10^{-17} \frac{D \rho r^2}{Q_{SW} \dot{M}_*} \ \ Myr. \tag{29}$$

Similarly to for PR drag, these time-scales can be compared to those for collisions equation (10) to derive a condition for the diameter below which particles are removed by stellar wind drag:

$$D_{SWPR} = 194 \frac{\dot{M}_*^2 r^{14/3} \frac{dr}{r}^2 Q_D^{*5/3} D_c}{M_{tot}^2 M_*^{8/3} e^{10/3}} \ \ m. \tag{30}$$

In Fig. 6, D_{SWPR} is compared to D_{bl}, D_{SW} and D_{PR} throughout the star's evolution. It shows that stellar wind drag is only important for the stronger mass-loss rates on the horizontal and AGBs, seen in Fig. 1. This is generally true for all disc and star parameters considered in this study.

The strong mass-loss rates, however, only act for a relatively short time-scale, shorter than collisional time-scales, such that D_{SWPR} actually overestimates the size objects that are removed by stellar wind drag. Fig. 8 shows the maximum diameter particle that can be removed by stellar wind drag for a disc around a $2.9 \, M_\odot$ star, given the finite AGB lifetime. For the smallest radii discs, since planetesimals up to D_c (1.9 km) are present in our model, almost

all the mass in the disc is removed by stellar wind drag during the AGB phase. However, the maximum diameter particle that can be removed for large radii discs is not much larger than the blow-out size.

Although the majority of the disc mass at the end of the AGB still lies within the main belt, our treatment of the effects of stellar mass loss does not include the fate of smaller bodies migrating inwards under stellar wind drag. This is the main difference between our work and numerical simulations such as Dong et al. (2010). Dong et al. (2010) also include the effect of planets on a planetesimal belt, including the trapping of planetesimals into mean motion resonances. Although our models do not include the flux from small bodies spiralling in under stellar wind drag in the calculation of the disc luminosities, the amount of material distributed between the inner edge of the belt and the star has been monitored. This will be discussed further in Section 5.2.3, in terms of the hot WD discs observed around some stars (see e.g. Farihi et al. 2009).

4.4.5 Sublimation

As the star evolves to higher luminosities particles heat up and may sublimate. For some ideal assumptions, the resulting rate of change of diameter, D (in m), is independent of the size (Jura 2008):

$$\frac{dD}{dt} = \frac{2\dot{\sigma}_0}{\rho} \sqrt{\frac{T_0}{T(t)}} e^{\frac{-T_0}{T(t)}}, \tag{31}$$

where T is the temperature, in K, $\dot{\sigma}_0 = 1.5 \times 10^{10} \, kg \, m^{-2} \, s^{-1}$ and T_0 is the composition-dependent sublimation temperature. For pure water ice $T_0 = 5530 \, K$ and for olivine $T_0 = 65\,300 \, K$, meaning that water ices sublimate at $\sim$110 K, whereas silicates only sublimate at $\sim$1300 K. Here we define the ice-line and silicate sublimation radius as the radius inside of which black bodies have temperatures hotter than this.

The change in the position of the ice-line and silicate sublimation radius as the star's luminosity changes is shown in Fig. 9. It can be seen that the silicate sublimation radius is always smaller than the discs considered in the current models, hence the sublimation of silicates can be ignored for the population of discs considered.

Temperatures hot enough for the sublimation of water ices, on the other hand, are found in debris discs around MS stars; for example sublimation of water ice is important for comets in our Solar system on orbits that approach the Sun within the ice-line
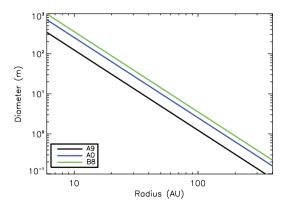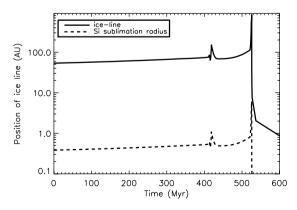

Figure 8. The maximum diameter object that can be removed by stellar wind drag, throughout the disc's evolution, ignoring collisions, as a function of disc radius, for a disc around a $1.67 \, M_\odot$ (A9), $2.9 \, M_\odot$ (A0) or $3.8 \, M_\odot$ (B8) star.

Figure 9. The change in position of the ice-line and silicate sublimation radius due to the change in luminosity of a $2.9 \, M_\odot$ star, $Z = 0.02$, as it evolves. Objects initially outside the ice-line on the MS, e.g. at 100 au, could end up inside of the ice-line around a giant or AGB star, such that any particles composed purely of water ice would sublimate.

of 6 au. A disc initially outside of the ice-line on the MS may be inside of it by either the giant or AGBs. The sublimation of objects composed entirely of water ice would therefore be expected, resulting in significant mass loss from objects of all sizes in the disc. Since sublimation loss time-scales are proportional to diameter, this means that smaller objects are removed most rapidly which could truncate the collisional cascade size distribution at a size larger than the blow-out limit.

However, the behaviour of more realistic objects of mixed composition is more complex. Sublimation may not proceed at the rate given by equation (31) indefinitely as water ice below the surface may be protected from sublimation by the surrounding layers of other non-volatile material (Jura & Xu 2010). As observed for Solar system comets, sublimation may also lead to the release of small dust grains that were originally embedded in the ice, thus increasing the number of small grains. Such a process was invoked in the models of Jura (2004). Thus, although sublimation may truncate the size distribution, and so reduce the number of small grains, it may also lead to the production of an extra population of small grains. Due to this complexity in behaviour, it is not clear that sublimation cleanly truncates the size distribution and it is therefore assumed not to dominate over other processes in the current models. Its effect is discussed further in Section 5.2.1.

4.4.6 Summary

The five processes that could potentially remove the smallest particles from the disc have been discussed. Fig. 6 provides a summary of which processes are relevant as the star evolves. Radiation pressure removes the largest particles from the disc throughout most of its evolution, apart from on the AGB when stellar mass-loss rates are high and relatively large objects are removed from the collisional cascade by stellar wind drag. PR drag is only relevant for small radii discs on the MS and giant branch. Uncertainties in the outcome of sublimation mean that the models presented in this paper assume that discs are unaffected by this process; the implications of this assumption are discussed in Section 5.2.1. The maximum of D_{bl}, D_{SWPR}, D_{PR} and D_{SW}, as shown in Fig. 6, was used to determine the cut-off of the collisional cascade, D_{min}, in our models. For epochs where D_{min} decreases with time, a time delay would be expected before the small grains are replenished by collisions. However in these models we assume that this delay is shorter than the time-scales considered and that the collisional cascade is instantaneously replenished. For example, at the start of the WD phase D_{min} decreases rapidly, however small grains will be replenished quickly by collisions. The collisional lifetime for small bodies is short, even though the collisional lifetime for the largest bodies in the disc is long (Section 4.2).
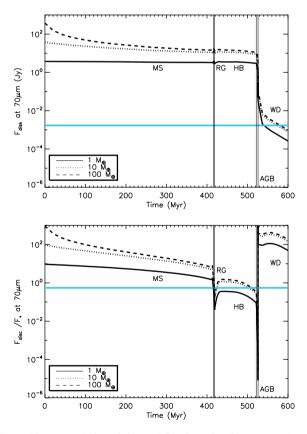
5 OBSERVATIONS

The preceding section discussed the various processes that affect the disc as the star evolves. Combining these processes, together with the knowledge of the change in stellar properties as the star evolves (Fig. 1), the evolution of a debris disc and its observable properties on the post-MS can be modelled. The evolution of an individual disc is, of course, dependent on its initial conditions, characterized in the current models by its radius, initial mass, distance from the Earth and the spectral type of the star. In this section we first consider the evolution of an individual disc, with a given set of parameters, and then proceed to discuss the evolution of the population of debris discs observed on the MS around A stars.

The two quantities of relevance to observations of the disc are its flux (F_{disc}) and the ratio of the flux from the disc to the flux from the star (R_ν). In order for a disc to be detected by a given instrument, at a given wavelength, its flux (F_{disc}) must be above the sensitivity limit for that instrument (F_{sens}), and the ratio of the flux from the disc to the flux from the star (R_ν) must be above the calibration limit ($R_{\nu,lim}$). The calibration limit is set by the accuracy that the stellar flux is known and the quality of the instrumental calibration. Here, it is assumed that all far-IR measurements have the same calibration limit as *Spitzer* at 70 μm (∼0.55), whilst mid-IR measurements, such as *Spitzer* at 24 μm, have a calibration limit of ∼0.1. Although the instrument calibration for *Herschel* is quoted as 0.1 (Poglitsch & Waelker 2010), once the uncertainty in the stellar flux is included the limit will be similar to that for *Spitzer* at 70 μm.

5.1 Evolution of a 100 au disc around a 2.9 M$_\odot$ star at a distance of 10 pc

Fig. 10 shows the evolution of F_{disc} and $R_{70\,\mu m}$ at 70 μm, for a disc initially at 100 au, with a mass of 1, 10 or 100 M$_\oplus$, around a 2.9 M$_\odot$ star at 10 pc. The blue lines show the sensitivity and calibration limits for *Spitzer* at 70 μm, respectively. The disc is detectable if both F_{disc} and $R_{70\,\mu m}$ are above these limits. From these plots, it can be seen that a disc of these initial conditions can be detected on the MS, early on the giant branch and early in the WD phase. The exact values of F_{disc} and $R_{70\,\mu m}$, relative to the calibration and

Figure 10. The evolution of the total flux from the disc (top panel) and the ratio of the flux from the disc to the flux from the star (middle panel) at 70 μm, as the star evolves. The thick blue line in the upper plot is the sensitivity limit of 110 μJy, whilst in the middle plot it shows the calibration limit of $R_{lim} = 0.1$, for *Spitzer* at 70 μm. The star is a 2.9 M$_\odot$ star, with solar metallicity $Z = 0.02$ at 10 pc and the disc has an initial radius of 100 au.

sensitivity limits, vary significantly for discs of different radius, initial mass, distance from the Earth or around different spectral-type stars; however the form of these plots, in terms of when F_{disc} and $R_{70\,\mu m}$ increase or decrease relative to the evolutionary phase of the star, remains relatively unchanged. The discussion begins below by considering the variation of F_{disc} and $R_{70\,\mu m}$ during the evolution of a disc with a given set of initial parameters and then goes on to consider the changes to this evolution when these initial parameters of the disc are varied in Sections 5.1.1, 5.1.2 and 5.1.3.

Along the MS, the stellar properties change only by a small amount and the evolution of the disc is unchanged from that in Wyatt et al. (2007). The flux from the disc falls off with time as collisional evolution depletes the mass in the disc. Observations of discs around nearby stars with *Spitzer* at 70 μm are in general calibration limited, and the example shown at 100 au is detectable throughout the MS.

On the giant branch, the stellar luminosity increases by several orders of magnitude (see Fig. 1). The increase in stellar luminosity heats the disc; however the increase in disc flux is small since all the small grains that would dominate the emission are removed by radiation pressure (see middle panel of Fig. 7). There is a substantial decrease in $R_{70\,\mu m}$ with time along the giant branch, since the increase in stellar flux is large, whilst the increase in F_{disc} on the giant branch is relatively small. The difficulty in observing discs around giant stars is therefore the calibration limit, as can be seen in Fig. 10 for the example disc for which $R_{70\,\mu m}$ is only greater than $R_{70\,\mu m,lim}$ for the first half of the star's giant branch evolution.

As the star moves on to the HB, its luminosity decreases from the maximum value on the giant branch, but remains higher than on the MS, whilst the stellar temperature remains low (see Fig. 1). The combination of these means that the stellar flux is high and $R_{70\,\mu m}$ is small, less than $R_{70\,\mu m,lim}$, for the $10\,M_\oplus$ example disc. This is true for the majority of discs in our population.

As helium in the core is exhausted, the star swells to become an AGB star. It ejects a significant proportion of its mass in a stellar wind and the smallest grains are removed by stellar wind drag ($D_{min} = D_{SWPR}$; equation 30). The stellar luminosity increases and heats the disc such that F_{disc} remains high, despite the fact that D_{min} is relatively large. This means that $R_\nu < R_{\nu,lim}$ and discs do not have an observable excess from a debris disc. However AGB stars may be surrounded by expanding circumstellar envelopes of material ejected from the star in a stellar wind, and emission from these dust shells would be significantly brighter than a debris disc in the infrared or sub-mm.

After mass loss ceases, the WD core evolves swiftly to higher effective temperature at constant luminosity, before the stellar luminosity starts to fall as the star cools as a WD. As the stellar luminosity decreases, R_ν increases and it becomes possible to detect emission from this example debris disc. For this short evolutionary epoch, the star is defined as a post-AGB or pre-WD. For the purposes of these models, we have defined the post-AGB phase as the 0.1 Myr before the start of the WD phase.

There is a sharp drop in stellar luminosity as the stellar envelope is ejected and the stellar core is exposed as a WD. This means that the ratio of the stellar luminosity to the disc flux increases significantly and that observations are no longer calibration limited. However, the disc flux falls rapidly below the sensitivity limit as the WD cools and it is this limit that determines whether a WD debris disc is detectable. As discussed in Section 4.4.1 even though there is no process to remove small dust created in collisions, the flux

from these small grains is small and does not make a WD debris disc detectable. As can be seen in Fig. 10, F_{disc} is only greater than F_{sens} for very young WDs.

5.1.1 Dependence on disc parameters

Changes in F_{disc} and R_ν with initial disc mass and radius are interlinked. Simplistically F_{disc}, and thus R_ν, is proportional to disc mass and hence discs that are more massive are easier to observe. The collisional evolution of material in the disc, however, means that there is a dependence of disc mass at later times on disc radius, since the collisional lifetime is shorter for close-in discs than for those further out (equation 10). For discs that have reached collisional equilibrium, their mass, at a given age, is independent of their initial mass but increases with disc radius (equation 12). Discs at large radii, on the other hand, will not have reached collisional equilibrium and so retain their initial mass. This leads to the behaviour of F_{disc} with radius shown in the upper panel of Fig. 11. For close-in discs the disc mass and thus F_{disc} increase with radius, despite the decrease in disc temperature. For large radii discs, on the other hand, there is a significant variation in F_{disc} with initial disc mass and F_{disc} decreases with radius or disc temperature. This behaviour is of particular importance in determining which radii discs are the brightest at a given epoch. As can be seen for a given individual disc mass, the brightest discs at some later epoch are those with intermediate radii at which the largest planetesimals are just reaching collisional equilibrium at this age.

5.1.2 Dependence on stellar parameters

The simplest scaling relation is the distance to the star. R_ν is unchanged, whilst F_{disc} scales inversely with distance squared. At large enough distances observations are always sensitivity limited.

In the current models stars with mass between 1.67 and $3.8\,M_\odot$ or spectral type A9–B8 are considered. The difference between these models that has the greatest effect on the disc is that in stellar luminosity. More luminous stars have brighter discs, although this increase is not as large as might be expected because the blow-out size also increases with stellar luminosity. Thus, the ratio of the disc flux to the stellar flux decreases with stellar luminosity, since the increase in stellar flux is larger than the increase in disc flux. In terms of Fig. 10 this means that, for higher luminosity stars, the upper plot is shifted upwards relative to the sensitivity limit, whilst the lower plot shifts downwards. As was discussed in Section 2, the stellar luminosity increases the most on the giant branch for lower mass stars, and therefore F_{disc} and R_ν show the greatest variation on the giant and AGB for these stars.

There is also a dependence in disc mass on MS lifetime for collisionally evolving discs. Later spectral-type stars take much longer to evolve and therefore the reduction in their disc mass at a given epoch is larger; however the difference in disc flux due to this is small compared to the difference due to the change in stellar luminosity.

In terms of detecting discs, this means that where observations are calibration limited, discs are more detectable around the least-luminous stars. This applies to lower mass stars on the MS, or early on the giant branch. On the other hand, when observations are sensitivity limited, i.e. around WDs, discs are more detectable around the most luminous, or higher mass stars.
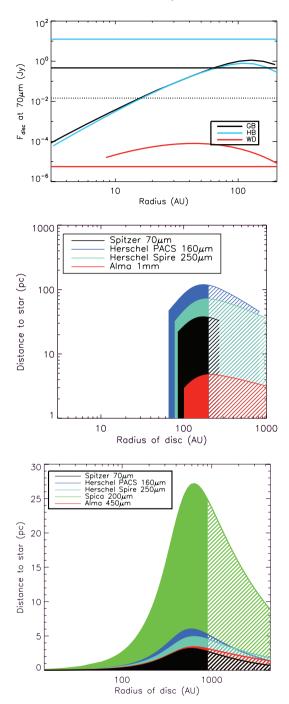
Figure 11. Observations of the disc. Upper: the variation in disc flux with radius for a 1.67 M$_\odot$ star on the giant branch (2000 Myr) (black line), HB (2200 Myr) (blue line) and around a WD (cooling age of 1 Gyr) (red line), for discs with an initial mass of 10 M$_\oplus$. The horizontal lines show the calibration limits for *Spitzer* at 70 μm on the giant branch (black), HB (blue) and WD phase (red), respectively, whilst the dotted horizontal line shows the sensitivity limit. Middle: detection limits for discs of initially 10 M$_\oplus$, around a star of 1.67 M$_\odot$, at the base of the giant branch ($L_* = 10.2$ L$_\odot$). Excesses can be observed for the discs that fall within the solid filled regions for *Herschel* PACS at 160 μm, *Herschel* SPIRE at 250 μm, Alma at 1 mm and *Spitzer* at 70 μm. The dashed filled regions are for discs with radii larger than 200 au, not included in the current models, that can be detected. A calibration limit of $R_{\nu,\text{lim}} = 0.55$ is assumed for all instruments. Lower: same as middle but for a 3.8 M$_\odot$ (equivalent to B8) star that has evolved to become a 1 Myr old WD. Note that the disc radii are 3.93 times larger than on the MS.

5.1.3 Dependence on wavelength of observations

The above discussion has focused on observations with *Spitzer* at 70 μm. The form of the upper and middle panels of Fig. 11 remains relatively unchanged as observations are made in different wavelengths; however the exact values of F_{disc} and R_ν relative to the sensitivity and calibration limits vary significantly. The disc flux peaks at approximately the peak emission wavelength for a blackbody of the disc temperature. The ratio of the disc to stellar flux also has a similar variation with wavelength; however it peaks at longer wavelengths, since F_* falls off more rapidly with wavelength than F_{disc}. Variations in F_{disc} and R_ν are larger for shorter wavelengths, where the emission is from the Wien region of the blackbody spectrum.

All of this behaviour means that there will be an optimum wavelength for detecting discs that depends on disc temperature, and whether observations are sensitivity or calibration limited. When observations are sensitivity limited, discs are most detectable for the wavelength at which F_{disc} is maximum, given by Wien's displacement law for a disc of a given temperature, around 100 μm for young WDs. Alternatively, when observations are calibration limited, the most discs are detectable for the wavelengths at which R_ν is maximum, for example on the giant branch this varies between 100 and 800 μm.

5.2 Population models

Using our models the evolution of a disc, with a given set of initial parameters, can be determined. Here, we apply these models to the population of discs on the MS known from observations of A stars by *Spitzer* and the models of Wyatt et al. (2007) (see Section 3). These discs are evolved from the MS through to the WD phase and the population of discs around evolved stars is determined. The following discussion focuses on giant stars, HB, post-AGB stars and WDs. AGB stars are not discussed because debris discs are not detectable during this phase, and in any case observations would be complicated by the presence of material emitted in the stellar wind.

There are many surveys for debris discs with recent and current instruments, such as *Spitzer* and *Herschel*, as well as upcoming instruments such as Alma. Here we calculate the percentage of the evolved population that are detectable with various instruments. Table 2 shows these percentages for young WDs, HB, giant and MS stars.

It is important to note that these percentages only correspond to the population of evolved A stars, not the entire population of giants, HB stars or WDs. The number of discs that these percentages correspond to can be calculated from the space density of A stars from Phillips et al. (2010) of 0.0014 ± 0.0001 pc^{-3} and the average MS lifetime for A stars, 950 Myr, to give a density of 3.5×10^{-5} pc^{-3} for evolved A stars on the giant branch, 2.5×10^{-4} pc^{-3} on the HB and 1.47×10^{-4} pc^{-3} for WDs with a cooling age of less than 100 Myr. It is not possible to tell from observations of giant stars whether they are evolved FGK or A stars, and it is therefore hard to compare the populations; however the majority of WDs currently observed are evolved A stars and these space densities make a reasonable comparison with the 80 per cent complete catalogue of Sion et al. (2009). The number of WDs within 10 pc less than 100 Myr old is predicted to be 0.6 and less than 1000 Myr within 20 pc is predicted to be 50, compared to 0 and 30 (Sion et al. 2009). This catalogue contains no WDs with cooling ages of less than 1 Myr with 20 pc.

Table 2. Detection of discs around evolved stars.

Instruments	Sensitivity (mJy)	Main sequence $d < 100$ pc (per cent)	Giant branch $d < 100$ pc (per cent)	Horizontal branch $d < 50$ pc $L < 100 \mathrm{L}_\odot$ (per cent)	Post-AGB $d < 200$ pc t_{WD}-0.1 Myr $< t < t_{WD}$ (per cent)	WD $d < 10$ pc $t_{WD} < 1000$ Myr
IRAS at 60 μm[a]	100[b]	4.6	1.7	0.6	1.8	<0.1
Spitzer at 24 μm	0.11[c]	51.0	14.0	20.5	<1.0	<0.1
Spitzer at 70 μm	14.4[c]	39.0	9.3	<1.0	6.3	<0.1
Spitzer at 160 μm	40[c]	13.0	4.2	1.0	5.7	<0.1
Herschel PACS at 70 μm	4[d]	44.0	9.6	<1.0	9.1	<0.1
Herschel PACS at 160 μm	4[d]	35.0	12.2	1.0	9.1	1.6
Herschel SPIRE at 250 μm	1.8[d]	33.0	12.8	2.5	22.6	1.9
Herschel SPIRE at 350 μm	2.2[d]	23.0	10.8	3.0	11.4	1.0
Alma at 450 μm	80[e]	19.0	7.0	3.0	12.6	1.1
Alma at 1.2 mm	0.25	10.7	2.2	<0.1	22.6	2.5
Spica at 200 μm	0.1[f]	45.0	12.0	1.5	22.6	23.70
No. of stars[g]		5860	1050	130	5.0	6.6

[a]Only stars with magnitudes brighter than 4.0 are considered such that the sample can be compared with Jura (1990).

[b]http://irsa.ipac.caltech.edu/IRASdocs/iras_mission.html

[c]Wyatt (2008).

[d]http://herschel.esac.esa.int/science_instruments.shtml

[e]http://www.eso.org/sci/facilities/alma/observing/specifications/

[f]Swinyard & Nakagawa (2009).

[g]The number of evolved A stars, calculated from the space density of A stars (Phillips et al. 2010).

5.2.1 Giant stars

Early on the giant branch a small set of the evolved population of debris discs has a detectable excess. The following discussion defines which discs are detectable, in terms of the parameter space specified by initial disc radius, initial disc mass, distance to the star, wavelength for observations and mass of the star. In order to assess this, the disc flux is plotted as a function of radius in the upper panel of Fig. 11. As discussed in Section 5.1.1, this peaks at intermediate radii because collisions have depleted the mass in close-in discs, such that $F_{disc} \propto M_{max} \propto r^{7/3}$ (equation 12), whereas large disc radii retain their initial masses, and the disc flux falls off with the disc temperature or radius. Only discs with $R_\nu > R_{lim}$ are detectable, or those with fluxes above the solid lines in the upper panel of Fig. 11, excluding both small and large radii discs.

This dependence leads to the form of the middle panel of Fig. 11, the solid area of which shows the discs that can be detected with various instruments. The upper curve is the sensitivity limit, whilst the cut-off at low and high radii is from the calibration limit. This plot varies with mass and age of the star, as well as mass of the disc and wavelength for observations. As can be seen for the example disc shown, around an evolved 1.67 M$_\odot$ star, of initially 10 M$_\oplus$ at the start of the giant branch, only discs with radii of around 100 au, within ~200 pc of the Sun, are detectable with *Spitzer*, *Herschel* or Alma at the wavelengths considered. As the luminosity of the star increases along the giant branch, the distance out to which discs can be detected increases; however the range of radii of discs with detectable excess decreases. This means that the solid (detectable) area of an equivalent to the middle panel of Fig. 11 is largest for the least-luminous giants. The dependence of disc flux on wavelength discussed in Section 5.1.3 means that the solid (detectable) area is largest for *Herschel* PACS at 160 μm.

A smaller fraction of the population has detectable excess on the giant branch than the MS, as can be seen in Table 2. The significant increase in stellar luminosity, compared to the small increase in disc flux, means that fewer discs are detectable over the stellar emission ($R_\nu > R_{lim}$). *Spitzer* at 24 μm can detect the largest fraction of the population, because observations are calibration limited and the calibration limit in the mid-IR is lower than in the far-IR. *Herschel* SPIRE detects the next highest fraction of the population due to the wavelength dependence of R_ν, peaking in the sub-mm, as discussed in Section 5.1.3. A sample of stars within 100 pc is considered in Table 2. However, if observations with, for example, Alma were made with the intention of detecting such discs, a sample that only extended out to smaller distances would maximize the rate of detection.

Our models suggest that around 10 per cent of evolved A stars on the giant branch have detectable excess with *Spitzer* or *Herschel*. This is, however, subject to the unclear effect of sublimation on debris discs. Sublimation could have two possible effects. Either it removes all small grains, truncating the collisional cascade, and thus decreasing the number of discs with detectable excess, or it releases a population of small silicate grains, increasing the number of giants with detectable excess. This makes future observations of giant stars with *Herschel*, in comparison with our models, very interesting, as they have the potential to constrain the effects of sublimation on discs.

Our models, however, compare favourably with the sample of 44 giants brighter than $m_v = 4.0$ mag (Jura 1990) (see Table 2), none of which displays excess at 60 μm (<3 per cent) with *IRAS*. Infrared excess is, however, found around 300 of the 40 000 G and K giants in the Bright Star Catalogue and Michigan Spectral Catalogue (Zuckerman, Kim & Liu 1995), although the origin of this emission is not clear. 12 of these sources are modelled in further detail in Kim et al. (2001), who suggest that they are more likely to result from sporadic dust ejection or emission from nearby interstellar cirrus rather than blackbody grains in a Kuiper-belt disc. In order to compare observations of giant stars with our models, it would be necessary to distinguish between these scenarios, potentially with high-resolution imaging.

Another factor that could significantly change the detectability of discs around giant stars is the radius distribution of discs in our population. Our models only included discs detected with *Spitzer* at 24 and 70 μm, and therefore there is a bias towards small radii discs. This is particularly relevant, as large radii discs are detectable, particularly at longer wavelengths (see middle panel of Fig. 11). This could be accounted for by extending our models to include sub-mm observations of debris discs on the MS or incorporating this radius bias into our modelling of the MS population. Including observations of discs around MS FGK stars would also make our models more directly comparable with a sample of giant stars. Given these extensions and a technique to distinguish emission from a debris discs from stars undergoing sporadic dust ejection or emission from nearby interstellar cirrus, it should be possible for future observations with *Herschel* or Alma to determine the effect of sublimation on debris discs.
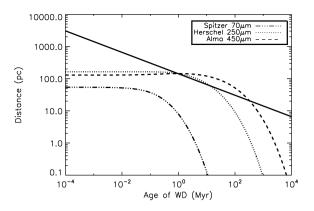
5.2.2 Horizontal branch stars

The majority of the discussion in Section 5.2.1 also applies to HB stars. Observations are also calibration limited; however significantly fewer discs are detectable around HB stars than giant stars, since the stellar flux is on average higher, whilst the disc flux remains approximately constant. In order to maximize the percentage of discs with detectable excess observations should focus on low-luminosity HB stars. In Table 2, the percentage of the population of HB stars within 20 pc and with luminosities lower than $100\,L_\odot$ were calculated. The most discs are detectable with *Herschel* PACS at 160 μm since this is the wavelength at which R_ν is maximum.

5.2.3 White dwarfs

As can be seen in Fig. 10, the disc flux falls off rapidly as the star cools during the WD phase and it is therefore very hard to detect debris discs around WDs. Observations of debris discs around WDs in our baseline model are sensitivity limited and only the most massive discs around the closest, youngest WDs are detectable. By the same analysis as in Section 5.2.1, the bottom panel of Fig. 11 shows the distance out to which discs of initially $10\,M_\oplus$ can be detected around an evolved $3.8\,M_\odot$ (equivalent to B8) star, with a WD cooling age of 1 Myr. Thus, for discs in our baseline model (initial radii less than 200 au) around WDs that are younger than 1 Myr, the disc flux is so low that it is only those that are within a couple of parsec of the Sun that are detectable with *Spitzer*, *Herschel* or Alma. Even the increased sensitivity of Spica only means that discs out to tens of parsec are detectable.

Similarly to discs around giant stars, it is the large radii discs that retain the highest mass at late times, that are therefore the most detectable. As can be seen in the upper panel of Fig. 11, F_{disc} peaks at ~200 au for a disc of initially $1\,M_\oplus$ around the 1 Myr old WD considered. This radius increases with initial disc mass or WD cooling age.

There is, however, a balance between young WDs being the most luminous and therefore having the brightest discs and the low-volume density of young WDs such that they are more likely to be found at greater distances from the Sun. Fig. 12 shows the maximum distance out to which discs around WDs can be detected as a function of cooling age, for discs at 100 au with *Spitzer* at 70 μm, *Herschel* SPIRE at 250 μm and Alma at 450 μm. This is compared to the distance within which one WD of a given cooling age is found, according to the space densities of Phillips et al.
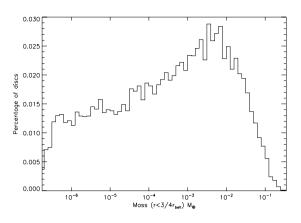

Figure 12. The solid line shows the maximum distance out to which a disc initially at 100 au, with a mass of $10\,M_\oplus$, around an evolved $3.8\,M_\odot$ WD, of a given age can be detected with *Spitzer* at 70 μm, *Herschel* at 250 μm and Alma at 450 μm, whilst the dotted line shows the distance within which there is one WD younger than the given age, calculated using the space density of A stars from Phillips et al. (2010).

(2010). The maximum distance out to which discs can be detected is never significantly greater than the distance within which there is one WD, and it is therefore unlikely that such a system can be observed. There is an optimum cooling age for detecting WD discs, which varies with wavelength, for *Spitzer* at 70 μm it is ~1 Myr, whilst for *Herschel* SPIRE at 250 μm it is ~10 Myr and for Alma at 450 μm it is ~100 Myr. As the disc temperature drops, the disc flux decreases, more rapidly at the shorter wavelengths. This means that for a young population of WDs, the best chances of detecting debris discs are at the shorter wavelengths of *Spitzer* or *Herschel*, whilst for a sample that includes older stars Alma would be better. However, overall, the best chances of detecting such a system are with the longer wavelengths of *Herschel* or Alma.

Focusing on *Spitzer* at 70 μm, if for some reason our models underpredicted the flux from (or mass in) such discs by approximately an order of magnitude, a disc would be most likely to be detected around a WD of less than 5 Myr old at a distance of around 200 pc. The only detection of excess around a WD that resembles a MS debris disc is the helix nebula (Su et al. 2007), a young WD with a cooling age significantly less than 5 Myr, surrounded by a planetary nebula at 219 pc. This fits nicely with our models, especially given that alternative explanations that increase the disc flux exist, for example the trapping of bodies in resonances (Dong et al. 2010).

There are very few young WDs close to the Sun, therefore assuming that our models are correct, the best chances of detecting a WD debris disc are to observe nearby WDs with Alma. Table 2 shows the percentage of the population of WDs within 10 pc with a cooling age of less than 1000 Myr. According to the space densities of Phillips et al. (2010), there are only six WDs in this distance, and even less from Sion et al. (2009), and therefore the chances of one of these WDs having a debris disc within the narrow initial radius and initial mass range such that it is detectable are slim. Increasing the distance limit of the sample does not improve matters as at greater distances the discs flux falls below the sensitivity limit. Even with the increased sensitivity of Spica the chances of observing such a disc around a WD are slim.

These low probabilities for detecting debris discs around WDs fit with the fact that *Spitzer* observations of WDs that have only found one WD with infrared excess fitted by a disc with a radius of the same order of magnitude of MS debris discs. There are, however, ~20 observations of hot, dusty discs around WDs that are best fitted by discs of radii of the order the solar radius (e.g. Reach et al. 2005;

Figure 13. A histogram showing the amount of mass left inside of the main belt (between $r = 0$ and $r = \frac{3}{4} r_{belt}$) at the end of the AGB for the population of discs in our models.

Farihi et al. 2009). Farihi et al. (2009) estimate that 1–3 per cent of WDs with cooling ages less than 0.5 Gyr possess hot IR excess. The minimum radius of a disc in our population is ~ 10 au, and therefore these observations cannot be explained by the discs in our population. Material in discs with such a small radius will have a very short lifetime and must, therefore, be replenished. Within the context of the current model we have identified a potential source of material for such discs. Stellar wind drag was included in the current models in as far as it truncates the collisional cascade on the AGB. Material that leaves the disc will spiral in towards the Sun, most of it being accreted on to the star during the AGB; however some mass will be left between the inner edge of the belt and the star, at the end of the AGB. Fig. 13 shows this mass for all the discs in our population. The masses in Fig. 13 are significantly higher than the typical dust masses for these hot discs; e.g. $3.3 \times 10^{-10} M_{\oplus}$ of GD166-58 (Farihi, Zuckerman & Becklin 2008), and there are even a significant proportion of the population with more mass than the largest such disc, GD362, with a mass of $0.017 M_{\oplus}$ (Jura et al. 2009). However, a mechanism is still required to move this material in closer to the star. This could potentially be scattering by planets inside of the disc or the dynamical effects of mass loss on the disc. The effects will be considered in more detail in a future work.

5.2.4 Post-AGB or pre-WD stars

As discussed earlier in Section 5.1.2, the stellar flux from AGB stars is so high that it is hard to detect emission from a debris disc. However, as the stellar luminosity starts to drop just before the start of the WD phase, it is possible to detect discs around a small proportion of stars (see Table 2). The analysis is very similar to that for young WD stars, discussed in the previous section. The only difference is that it is possible to observe discs around somewhat more distant stars; however since the post-AGB phase is shorter the density of such stars is lower. The chances of detecting such a system are therefore slim. Many post-AGB stars have IR excess that can be modelled as a stable Keplerian disc (see van Winckel 2003 for a review). However, these discs are orders of magnitude brighter than a debris disc at this epoch and are most likely to be connected with binarity (Van Winckel 2007).

6 CONCLUSIONS

This work provides a theoretical framework that considers all of the effects of stellar evolution on debris discs, first considering the

evolution of an individual disc, before extending this to the known population of debris discs around MS A stars. It is found that debris discs are harder to detect around evolved stars than on the MS. The fraction of discs with detectable excess decreases significantly on the giant branch, yet further on the HB and discs around WDs are very hard to detect, although the limitations during this phase are different to earlier in the star's evolution.

The population of discs on the MS is constrained by *Spitzer* observations of A stars (Rieke et al. 2005; Su et al. 2006) and the steady-state collisional models of Wyatt et al. (2007). In this work these models were updated to include realistic grains rather than the blackbody approximation used in Wyatt et al. (2007). This was done relatively simplistically by considering that the difference in behaviour between realistic and blackbody grains can be explained entirely by an altered disc radius, characterized by the ratio X_{2470} between the radius calculated using realistic grains (r) and the radius calculated using a blackbody approximation (r_{2470}), shown in Fig. 3. This was used to adjust the fit from Wyatt et al. (2007), and thus the population of discs around MS A stars was determined.

In our models debris discs that are observed on the MS survive the star's evolution; however their properties are altered. They evolve collisionally in exactly the same manner as on the MS; however the longer time-scales mean that, except for large radii discs, their masses are significantly reduced. Discs heat up as the stellar luminosity increases on the giant and AGBs. The increase in disc flux, however, is relatively small since small grains are removed by radiation pressure and stellar wind drag (on the AGB only). It is shown that PR drag is irrelevant for all discs, including discs around WDs, the only exception being for low-mass or close-in discs. Adiabatic stellar mass loss means that discs around WDs have radii a factor of 2 or 3 greater than on the MS.

All of these changes in the properties of the disc can be put together to determine which discs can be detected. In terms of observations of discs around post-MS stars, the important quantities are the disc flux F_{disc} and its ratio to the stellar flux, R_{ν}, which must, respectively, be above the sensitivity and calibration limits of the instrument considered. The variation in these are summarized in Fig. 10.

A smaller fraction of the population can be detected on the giant branch than the MS. Observations are calibration limited. The large increase in stellar flux at the wavelengths considered, compared to the smaller increase in disc flux, means that R_{ν} decreases significantly and discs are hard to observe. R_{ν} decreases with time on the giant branch such that only large radii discs around stars early on the giant branch have a detectable excess. One limitation of our models is the uncertainty in the effect of sublimation on the disc, as discussed in Section 4.4.5. Future observations of giant stars with *Herschel* or Alma, in comparison with our models, could potentially constrain the effects of sublimation on debris discs.

Discs around WDs are very faint and thus hard to observe. Their luminosity decreases as the stellar luminosity falls off with age and the best chances of observing a disc are around very young WDs close to the Sun; however there are very few such objects and thus the chances of observing such a system are small. If for some reason our models underpredict the flux from such discs, then the optimum age and distance for detecting a WD disc with *Spitzer* at 70 μm would be at a distance of ~ 200 pc and an age of less than 5 Myr. This fits nicely with the one detected disc around WD 2226-210, the young WD at the centre of the helix nebula, at a distance of 219 pc (Su et al. 2007).

There are, however, detections of hot dusty discs around ~ 20 WDs with radii less than 0.01 au. These are a different

population from the discs in our models which have a minimum radius of 6 au. Within the context of our models a potential source of material to replenish such discs is material that has left the disc due to stellar wind drag, but not yet been accreted on to the star at the end of the AGB. However, a mechanism is still required to move this material in towards the star. This, and the dynamical effects of mass loss on debris discs, will be the subject of future work.

ACKNOWLEDGMENTS

REFERENCES

Andrews S. M., Williams J. P., 2005, ApJ, 631, 1134
Aumann H. H. et al., 1984, ApJ, 278, L23
Burns J. A., Lamy P. L., Soter S., 1979, Icarus, 40, 1
Dong R., Wang Y., Lin D. N. C., Liu X., 2010, ApJ, 715, 1036
Farihi J., Zuckerman B., Becklin E. E., 2008, ApJ, 674, 431
Farihi J., Jura M., Zuckerman B., 2009, ApJ, 694, 805
Hurley J. R., Pols O. R., Tout C. A., 2000, MNRAS, 315, 543
Jura M., 1990, ApJ, 365, 317
Jura M., 1999, ApJ, 515, 706
Jura M., 2004, ApJ, 603, 729
Jura M., 2008, AJ, 135, 1785
Jura M., Xu S., 2010, ApJ, preprint (arXiv e-prints)
Jura M., Muno M. P., Farihi J., Zuckerman B., 2009, ApJ, 699, 1473
Kennedy G. M., Wyatt M. C., 2010, MNRAS, 405, 1253
Kenyon S. J., Bromley B. C., 2004, ApJ, 602, L133
Kim S. S., Zuckerman B., Silverstone M., 2001, ApJ, 550, 1000
Kobayashi H., Tanaka H., 2010, Icarus, 206, 735
Krivov A. V., Müller S., Löhne T., Mutschke H., 2008, ApJ, 687, 608
Kudritzki R. P., Reimers D., 1978, A&A, 70, 227
Kurucz R. L., 1979, ApJS, 40, 1
Li A., Greenberg J. M., 1997, A&A, 323, 566
Löhne T., Krivov A. V., Rodmann J., 2008, ApJ, 673, 1123

Mestel L., 1952, MNRAS, 112, 583
Metcalfe T. S., Montgomery M. H., Kanaan A., 2004, ApJ, 605, L133
Mustill A., Wyatt M., 2009, MNRAS, 399, 1403
Olofsson H., Maercker M., Eriksson K., Gustafsson B., Schoier F., 2010, preprint (arXiv e-prints)
Phillips N. M., Greaves J. S., Dent W. R. F., Matthews B. C., Holland W. S., Wyatt M. C., Sibthorpe B., 2010, MNRAS, 403, 1089
Plavchan P., Werner M. W., Chen C. H., Stapelfeldt K. R., Su K. Y. L., Stauffer J. R., Song I., 2009, ApJ, 698, 1068
Poglitsch A., Waelker C., 2010, A&A, 518, L2
Reach W. T., Kuchner M. J., von Hippel T., Burrows A., Mullally F., Kilic M., Winget D. E., 2005, ApJ, 635, L161
Rieke G. H. et al., 2005, ApJ, 620, 1010
Sion E. M., Holberg J. B., Oswalt T. D., McCook G. P., Wasatonic R., 2009, AJ, 138, 1681
Strubbe L. E., Chiang E. I., 2006, ApJ, 648, 652
Su K. Y. L. et al., 2006, ApJ, 653, 675
Su K. Y. L., Chu Y.-H., Rieke G. H., Huggins P. J., Gruendl R., Napiwotzki R., Rauch T., Latter W. B., Volk K., 2007, ApJ, 657, L41
Su K. Y. L. et al., 2009, ApJ, 705, 314
Swinyard B., Nakagawa T., 2009, Exp. Astron., 23, 193
Thébault P., Augereau J., 2007, A&A, 472, 169
van Winckel H., 2003, ARA&A, 41, 391
Van Winckel H., 2007, Baltic Astron., 16, 112
van Winckel H. et al., 2009, A&A, 505, 1221
Vassiliadis E., Wood P. R., 1993, ApJ, 413, 641
Villaver E., Livio M., 2007, ApJ, 661, 1192
von Hippel T., Kuchner M. J., Kilic M., Mullally F., Reach W. T., 2007, ApJ, 662, 544
Willson L. A., 2000, ARA&A, 38, 573
Wyatt M. C., 2005, A&A, 433, 1007
Wyatt M. C., 2008, ARA&A, 46, 339
Wyatt M. C., Dent W. R. F., 2002, MNRAS, 334, 589
Wyatt M. C., Smith R., Su K. Y. L., Rieke G. H., Greaves J. S., Beichman C. A., Bryden G., 2007, ApJ, 663, 365
Zuckerman B., Kim S. S., Liu T., 1995, ApJ, 446, L79

This paper has been typeset from a TEX/LATEX file prepared by the author.